

AUTHOR QUERY FORM

	<p>Journal: J. Chem. Phys.</p> <p>Article Number: JCP22-AR-NUCL2022-04263</p>	<p>Please provide your responses and any corrections by annotating this PDF and uploading it to AIP's eProof website as detailed in the Welcome email.</p>
---	---	--

Dear Author,

Below are the queries associated with your article. Please answer all of these queries before sending the proof back to AIP.

Article checklist: In order to ensure greater accuracy, please check the following and make all necessary corrections before returning your proof.

1. Is the title of your article accurate and spelled correctly?
2. Please check affiliations including spelling, completeness, and correct linking to authors.
3. Did you remember to include acknowledgment of funding, if required, and is it accurate?

Location in article	Query/Remark: click on the Q link to navigate to the appropriate spot in the proof. There, insert your comments as a PDF annotation.
Q1	Please check that the author names are in the proper order and spelled correctly. Also, please ensure that each author's given and surnames have been correctly identified (given names are highlighted in red and surnames appear in blue).
Q2	In sentence beginning "To do that..." please confirm that "following section" refers to Sec. III B 2.
Q3	Figures must be cited in numerical order; therefore, we have renumbered Figs. 4 and 3 as 3 and 4. Please check.
Q4	In sentence beginning "By fitting $\gamma(p)$..." please confirm that "following section" refers to Sec. III B 4.
Q5	Please confirm the change in author's initials in Refs. 1, 3, 16, 28, 31, 32, 52, 61, and 69.
Q6	Please confirm the change in page number in Ref. 20.
Q7	Please update Ref. 33 with volume number, page number, and year if published. If not yet published, please provide the article title and, if available, the journal title. If the article is an "early" or "advance" view published online by a journal before assignment to a volume and issue, please provide a DOI if available.
Q8	References 36 and 38 contain identical information. Please check and provide the correct reference or delete the duplicate reference. If the duplicate is deleted, renumber the reference list as needed and update all citations in the text.
Q9	We were unable to locate a digital object identifier (doi) for Refs. 48 and 49. Please verify and correct author names and journal details (journal title, volume number, page number, and year) as needed and provide the doi. If a doi is not available, no other information is needed from you. For additional information on doi's, please select this link: http://www.doi.org/ .
Q10	If e-print Ref. 58 has subsequently been published elsewhere, please provide updated reference information (journal title, volume number, and page number).

Continued on next page

Continued from previous page

Q11

Please provide publisher's name in Ref. 73.

Please confirm ORCID's are accurate. If you wish to add an ORCID for any author that does not have one, you may do so now. For more information on ORCID, see <https://orcid.org/>.

Cintia P. Lamas – 0000-0001-9453-1205

Carlos Vega – 0000-0002-2417-9645

Eva G. Noya – 0000-0002-6359-1026

Eduardo Sanz – 0000-0001-6474-5835

Please check and confirm the Funder(s) and Grant Reference Number(s) provided with your submission:

Ministerio de Ciencia e Innovación, Award/Contract Number PID2019-105898GB-C21

Agencia Estatal de Investigación, Award/Contract Number PID2020-115722GB-C21

Ministerio de Universidades, Award/Contract Number FPU18/03326

Please add any additional funding sources not stated above.

Thank you for your assistance.

Author Proof

The water cavitation line as predicted by the TIP4P/2005 model

Cite as: J. Chem. Phys. 158, 000000 (2023); doi: 10.1063/5.0139470

Submitted: 20 December 2022 • Accepted: 14 February 2023 •

Published Online: 9 99 9999



View Online



Export Citation



CrossMark

Cintia P. Lamas,^{1,2} Carlos Vega,¹ Eva G. Noya,² and Eduardo Sanz^{1,a)}

AFFILIATIONS

¹Departamento de Química-Física I (Unidad de I+D+i Asociada al CSIC), Facultad de Ciencias Químicas, Universidad Complutense de Madrid, 28040 Madrid, Spain

²Instituto de Química Física Rocasolano, CSIC, C/ Serrano 119, 28006 Madrid, Spain

Note: This paper is part of the JCP Special Topic on Nucleation: Current Understanding Approaching 150 Years After Gibbs.

^{a)}Author to whom correspondence should be addressed: esa01@ucm.es

ABSTRACT

The formation of vapor bubbles in a metastable liquid, cavitation, is an activated process due to the free energy cost of having both phases at contact. Such an energetic penalty enables the existence of the liquid beyond its thermodynamic borders. Establishing the stability limits of a liquid as ubiquitous as water has important practical implications and has thereby attracted a lot of attention. Different experimental strategies and theoretical analyses have been employed to measure and predict the cavitation line, or the pressure–temperature kinetic stability border of liquid water. Understanding the location of the cavitation line requires knowing the cavitation rate dependence on pressure and temperature. Such dependency is difficult to obtain in experiments, and we use molecular simulations with the TIP4P/2005 model to fill this gap. By deeply overstretching liquid water below the saturation pressure, we are able to observe and quantify spontaneous cavitation. To deal with a lower overstretching regime, we resort to the Seeding technique, which consists of analyzing simulations of a liquid containing a vapor bubble under the theoretical framework of Classical Nucleation Theory. Combining spontaneous cavitation with Seeding, we get a wide overview of the cavitation rate along with pressure. We study two different temperatures (450 and 550 K) and complement our perspective with the results previously obtained at 296.4 K [Menzl *et al.*, Proc. Natl. Acad. Sci. **113**, 13582 (2016)] to establish a broad simulation-experiment comparison. We find a good agreement between simulations and both isobaric heating and isochoric cooling experiments using quartz inclusions. We are, however, unable to reconcile simulations with other experimental techniques. Our results predict a decrease in the solid–liquid interfacial free energy as the liquid becomes increasingly overstretched with a temperature independent Tolman length of 0.1 nm. Therefore, the capillarity approximation underestimates the nucleation rate. Nonetheless, it provides a fair indication of the location of the cavitation line given the steep rate vs pressure dependence. Overall, our work provides a comprehensive view of the water cavitation phenomenon and sets an efficient strategy to investigate it with molecular simulations.

Published under an exclusive license by AIP Publishing. <https://doi.org/10.1063/5.0139470>

I. INTRODUCTION

Many microwave ovens display a sticker with a symbol recommending placing a spoon in the mug where water is heated. The spoon acts as a surface to aid the emergence of vapor bubbles. When bubbles are formed, a liquid–vapor equilibrium is established, and heat transferred by microwaves is employed in increasing the number of molecules in the vapor phase rather than in a further temperature raise. In the absence of a spoon, however, bubbles may not form, and the liquid may get superheated beyond the boiling temperature. In such cases, water can boil explosively when handled by

the user. Superheating is not the only manner to have metastable liquid water with respect to the vapor. Metastability can also be achieved by overstretching the liquid below the vapor saturation pressure. This route enables probing negative pressures, which is of great interest for the study of the thermodynamic behavior of liquid water and the understanding of its anomalies.^{1–4} The emergence of vapor cavities in the metastable liquid (cavitation) sets the limit for the superheating or the overstretching that the liquid can sustain. Cavitation plays an important role in many industrial, technological, and geological processes,^{5–11} which makes the understanding of the physics that governs it of paramount importance.

This interest has prompted numerous experimental studies of water cavitation where vapor bubbles arise upon isobaric heating,¹² application of acoustic waves,^{13,14} or isochoric cooling.^{1,15–18} In these experiments, the metastability limit of the liquid with respect to the vapor is determined. The boundary between the metastable liquid and the vapor is a cavitation line in the pressure–temperature plane below which bubbles readily nucleate.^{1,19,20} This cavitation line is analogous to the so-called homogeneous ice nucleation line,²¹ which sets the temperature boundary (along pressure) for the metastability of the liquid with respect to ice. In both metastability situations (liquid vs vapor and liquid vs solid), it is the unfavorable interfacial free energy between the emerging phase (vapor or ice) and the surrounding liquid that enables the survival of the latter beyond its thermodynamic stability limits.^{22,23}

Experimental investigations on cavitation have been complemented by theoretical work in the framework of Classical Nucleation Theory (CNT)^{2,24,25} or, more recently, Density Functional Theory,²⁰ with the aim of predicting and understanding the location of the cavitation line. The agreement between theoretical predictions and experiments is quite satisfactory^{1,19,20} if the interfacial free energy between the liquid and the vapor is allowed to decrease when moving away from coexistence.^{2,20}

An important drawback of both theory and experiments is that they do not have access to detailed information at the molecular scale. For instance, the critical bubble (that has a 50% chance of either growing or redissolving) cannot be visualized experimentally due to its small size and short lifetime. Computer simulations can bridge this gap, and they have been extensively used to study cavitation in model systems like the Lennard–Jones fluid.^{26–33} Simulation work for water cavitation is more scarce, although due to the technical difficulty of studying a rare event like cavitation—which requires the use of special simulation methods—in a costly system from a computational point of view due to the presence of electrostatic interactions. Reference 3 pioneers in the simulation work on water cavitation. With the use of biased simulations that promoted the appearance of bubbles in the overstretched liquid, the authors of Ref. 3 were able to calculate the nucleation rate vs the liquid pressure for temperature $T = 296.4$ K. The nucleation rate—the number of critical bubbles that appear per unit of time and volume—is the central parameter in nucleation. By knowing the nucleation rate, one can estimate the pressure at which cavitation is going to take place in a certain experimental setup, which means that one can predict the location of the cavitation line. In fact, the authors of Ref. 3 report a cavitation pressure of -126 MPa at the studied temperature and for the selected water model (TIP4P/2005³⁴), which is in line with the measurements obtained in isochoric cooling in quartz inclusions,^{1,15} although at odds with acoustic cavitation experiments.^{14,35–38}

In this paper, we revisit the cavitation of overstretched water with simulations using the TIP4P/2005 water model.³⁴ We focus on two different temperatures as compared to Ref. 3, namely 450 and 550 K, enabling a more direct comparison with the regime where most experimental points of the homogeneous cavitation line are available. Moreover, we use an efficient computational approach based on directly simulating the liquid with a vapor bubble already formed at the beginning of the simulations.^{39–41} This strategy, called Seeding,^{29,42–46} combines average properties obtained in the simulations of the vapor bubbles with the theoretical formalism of CNT.^{47–49} We complement Seeding with unbiased

“brute force” molecular simulations in a high overstretching regime where bubbles appear spontaneously. Although such a regime is not attainable in experiments, we use brute force results to validate Seeding simulations that do overlap with experimentally relevant conditions.

Our simulation results for the location of the homogeneous cavitation line compare satisfactorily with theoretical predictions^{20,25} and experimental measurements.^{1,15} Simulated bubbles have an interfacial thickness of about 1 nm for 450 K and 2 nm for 550 K. The equi-density²⁸ definition of the bubble radius gives a better consistency between Seeding and Brute Force simulations than the Gibbs equi-molar surface. The interfacial free energy decreases as vapor bubbles become smaller (or as pressure decreases), which is inferred from our simulations. We also find that the vapor bubble pressure obtained by equating its chemical potential to that of the surrounding liquid is consistent with that given by the density in the interior of the bubble. This result, although expected, is not verified in liquid-to-solid phase transitions.^{50–52} Overall, our work shows that water cavitation can be studied from a molecular perspective, giving experimentally relevant information in a rather efficient manner.

II. SIMULATION DETAILS

We use the TIP4P/2005 force field for water, which is a rigid model consisting of three fixed point charges and one Lennard–Jones (LJ) center.³⁴

Molecular dynamics simulations are performed with the GROMACS package 2018 (single precision).⁵³ When simulating in the NpT ensemble, we use the Parrinello–Rahman barostat,⁵⁴ with a relaxation time of 2 ps and a compressibility of 10^{-5} bar⁻¹. To control the temperature, we use the Nosé–Hoover thermostat⁵⁵ with a relaxation time of 2 ps. For the Verlet integration of the equations of motion, we use a time step of 2 fs. To deal with electrostatic interactions, we use particle mesh Ewald summations.⁵⁶ The cut-off radius for the neighbor list, the dispersive Lennard–Jones interactions, and the real part of the electrostatic interactions are 13 Å. Ewald summations have been previously used to deal with heterogeneous systems,⁵⁷ including water bubbles.^{3,58} We have checked for specific cases of bubble simulations that the energy barely changes by increasing the Ewald cutoff to 20 Å. Moreover, we find that even using a plain 20 Å cutoff for the electrostatic interactions does not almost change the average energy. These arguments give us confidence in the use of Ewald summations with the selected 13 Å real part cutoff. No tail corrections are added to the Lennard–Jones potential due to the presence of two phases with strongly different densities in our simulations. We use a switch radius of 12 Å, meaning that the LJ potential is not modified up to this radius, after which it is gradually switched off to reach zero at the cut-off radius. The LINCS algorithm is used to fix the geometry of the water molecules, with an order of six and four iterations.^{59,60}

III. RESULTS

Most results discussed below correspond to a temperature of 450 K. Only at the end, in Sec. III B 5, we add results corresponding to 550 K in order to establish a broader comparison with experiments.

A. Coexistence properties

The liquid–vapor equilibrium for this model has been characterized in Ref. 61. We recalculate here the coexistence pressure at $T = 450$ K to both test our simulation setup and to account for the use of a slightly different cutoff radius. We first equilibrate a liquid of 4096 water molecules in a cubic box in the NpT ensemble. After, we introduce some empty space next to the liquid, finishing with a box of $3.917\,24 \times 3.917\,24 \times 27.14$ nm³. We run this system (in the NVT ensemble) until equilibrium has been reached and obtain the pressure components of the system. The pressure component normal to the vapor–liquid interface is the vapor (or coexistence) pressure, and it does not depend on the system size; in our case, $p_z = 4.49$ bar, in very good agreement with the values reported in Ref. 61 (4.46 bars) and Ref. 62 (4.5 bars). The tangential components of the pressure depend on the system size and in our case are $p_x = -24.38$ bars and $p_y = -24.48$ bars. The interfacial free energy at coexistence, γ_c , is obtained using the mechanical route,⁶³

$$\gamma_c = \frac{L_z \left[p_z - \frac{p_x + p_y}{2} \right]}{2}. \quad (1)$$

We obtain $\gamma_c = 40(1)$ mJ m⁻², which is similar to the value calculated in Ref. 62, $\gamma_c = 38.8$ mJ m⁻².

B. Cavitation rate

1. Cavitation rate by brute force molecular dynamics simulations

By lowering the pressure of the liquid below the coexistence value, one should observe the nucleation of vapor cavities (cavitation). Owing to the liquid–vapor interfacial free energy, this process is activated and can take a long time. At very low pressures, however, the thermodynamic drive for the emergence of the vapor phase is high, and the cavitation process is relatively quick. In fact, it is possible to observe it in brute force molecular dynamics simulations of the bulk liquid for negative pressures below -650 bar. This is shown in Fig. 1, where we plot the volume of the simulation box vs time for ten different trajectories starting from a bulk liquid consisting of 20 000 water molecules under periodic boundary conditions at 450 K and -700 bar. In all runs, the system abruptly increases its volume after some induction period (which varies stochastically from one trajectory to another) due to the sudden appearance and growth of a vapor bubble. The stochastic character of cavitation is a consequence of its activated nature. The fact that there is a long induction period indicates that a single bubble is formed in the system (an unlikely event does not happen twice or more at the same time). This enables us to estimate the bubble nucleation rate as

$$J = \frac{1}{\langle t \rangle \langle V \rangle}, \quad (2)$$

using 1 in the numerator because one only bubble forms in each run. $\langle t \rangle$ is the average time that it takes to observe the nucleation of a bubble, which is obtained as the arithmetic average between the times at which the volume sharply shoots up in our ten trajectories. $\langle V \rangle$ is the average volume of the liquid where bubble nucleation takes place. In Table I, we report the nucleation rates for different pressures alongside the variables required to compute them. Obviously, the lower

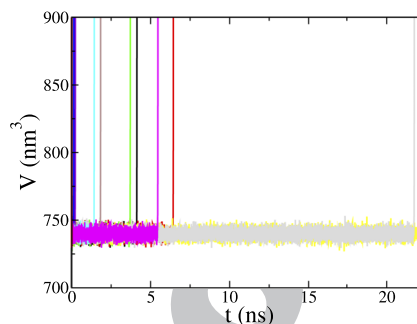


FIG. 1. Volume of the simulation box vs time starting from ten liquid configurations containing 20 000 molecules. The thermodynamic state point is 450 K and -700 bar.

the pressure, the higher the cavitation rate. With our brute force calculations, we span three orders of magnitude of the nucleation rate: from 10^{33} m⁻³ s⁻¹ at -750 bar to 10^{30} m⁻³ s⁻¹ at -650 bar. Probing lower nucleation rates with brute force calculation is too demanding computationally. It is important, however, to get estimates of lower nucleation rates given that in experiments one has access to rates of the order of Ref. 20 10^{15} m⁻³ s⁻¹. To do that, we resort to the Seeding technique, which is described in Sec. III B 2.

2. Cavitation rate via NVT Seeding

We shall compute the nucleation rate for higher pressures (lower rates) using Seeding.^{42–46} In this method, instead of waiting for a bubble to spontaneously appear, the simulation is started from a configuration of a liquid containing a bubble. When equilibrated in the NVT ensemble, the bubble turns out to be the critical vapor nucleus at the simulation temperature and at the pressure acquired by the surrounding liquid.²⁹ With such pressure and the bubble radius, one can obtain an estimate of the nucleation rate using CNT.²⁹

To prepare the initial configuration, we first equilibrate liquid water in the NpT ensemble at 450 K and a selected pressure below saturation. Next, we remove the molecules inside a sphere in the center of the box. This system is then simulated in the NVT ensemble and allowed to equilibrate during 1 ns. We repeat this process with different pressures, box sizes, and cavity radii looking for trajectories having a stable vapor bubble (stabilizing spherical nuclei in the NVT ensemble is not always viable and depends on a subtle balance between the size of the box and that of the nucleus^{29,51}). In Table II, we summarize the system sizes employed in our Seeding simulations

TABLE I. Data leading to the calculation of J via brute force molecular dynamics simulations using a system of 20 000 TIP4P/2005 water molecules at 450 K.

p (bar)	$\langle t \rangle$ (ns)	$\langle V \rangle$ (nm ³)	J (s ⁻¹ m ⁻³)
-750	0.5(2)	747.8(1)	$3(1) \times 10^{33}$
-725	1.1(2)	743.73(6)	$1.2(2) \times 10^{33}$
-700	7(3)	739.81(3)	$2.0(8) \times 10^{32}$
-675	40(10)	736.15(1)	$3.1(8) \times 10^{31}$
-650	300(100)	732.798(7)	$4(2) \times 10^{30}$

TABLE II. Data corresponding to the different NVT Seeding simulations performed in this work. See the main text for the meaning of the different reported parameters.

<i>T</i> (K)	<i>N</i>	<i>L</i> (nm)	<i>p_l</i> (bar)	Δp (bar)	ρ_l (kg/m ³)	ρ_v (kg/m ³)	<i>R_{ed}</i> (nm)	<i>R_G</i> (nm)	$\log_{10}[J_{ed}/(s^{-1} m^{-3})]$	$\log_{10}[J_G/(s^{-1} m^{-3})]$
450	58 817	13.9305	-135.4	142.2	869.8	3.79	5.43	5.46	-293	-299
	64 085	13.9305	-150.4	156.9	868.6	3.65	4.88	4.92	-227	-233
	47 110	12.3315	-190.8	196.8	865.2	3.34	3.85	3.89	-124	-130
	49 774	12.3315	-225.5	231.2	862.2	3.13	3.24	3.29	-75	-80
	49 774	12.3315	-226.2	231.9	862.2	3.12	3.24	3.29	-75	-80
	51 785	12.3315	-295.4	300.6	856.0	2.79	2.45	2.50	-24	-29
	17 985	8.8216	-308.7	313.7	854.8	2.73	2.33	2.39	-17	-22
	18 548	8.8056	-391.0	395.6	847.0	2.44	1.80	1.88	7	2
	18 524	8.8023	-391.0	395.6	847.0	2.44	1.80	1.88	7	2
	8 950	6.9651	-435.5	439.8	842.6	2.31	1.58	1.69	15	9
550	50 691	13.1049	-73.2	110.9	710.2	20.92	2.93	3.05	7	2
	17 064	9.2936	-86.4	123.7	706.6	20.56	2.55	2.70	16	11
	17 737	9.2936	-116.4	152.8	697.8	19.78	1.99	2.18	26	21

alongside the radii of the stabilized bubbles averaged over 19 ns. We report two different radii for each bubble. One is *R_G*, the radius corresponding to the equi-molar Gibbs dividing surface, which is computed as follows:

$$R_G = \left(\frac{3(N - L^3 \rho_l)}{4\pi(\rho_v - \rho_l)} \right)^{1/3}, \quad (3)$$

where *N* is the total number of molecules, *L* is the length of the simulation box edge (since we work with a cubic system the volume of the box is *L*³), and ρ_l and ρ_v are the densities of the liquid and the vapor phases, respectively. The former is obtained via the average virial pressure, *p_l*, and the bulk liquid equation of state (see Table II). The latter is obtained by looking for the vapor that has the same chemical potential as the surrounding liquid: $\mu_l(T, p_l) = \mu_v(T, p_v)$. We search where this condition is satisfied by performing isothermal thermodynamic integration of both the bulk vapor and the bulk liquid molar volumes from the coexistence pressure, *p_{coex}*, as described

in Ref. 28. In Fig. 2, we show $\mu(p) - \mu(p_{coex})$ at 450 K for the liquid (black curve) and the vapor (red curve). The dotted vertical line at *p* = -295.4 bar corresponds to *p_l* for a bubble of 2.5 nm. The chemical potential of such liquid can be obtained from the intersection between the dotted line and the black curve. Then, we read from the intersection between the horizontal dashed line and the red curve, the pressure of the vapor that has the same chemical potential as the liquid, *p_v*. Δp , a key parameter in the CNT nucleation formalism, is the difference between *p_v* and *p_l*. The vapor pressures, *p_v*, and the corresponding densities, ρ_v , thus obtained for all simulated bubbles, are reported in Table II.

Alternatively, we compute the bubble radius by means of an average radial density profile starting from the bubble center, as shown in Fig. 3. Such a density profile is fitted to the following sigmoid function (dashed orange curve in Fig. 3):

$$\rho(r) = \frac{\rho_{v,dp} + \rho_{l,dp}}{2} + \left(\frac{\rho_{l,dp} - \rho_{v,dp}}{2} \right) \cdot \tanh[(r - R_{ed})/\alpha], \quad (4)$$

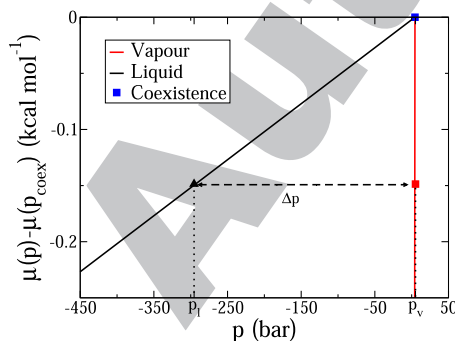


FIG. 2. Chemical potential difference with respect to the coexistence pressure at 450 K for the bulk liquid (black) and the bulk vapor (red) phases. Dashed and dotted horizontal and vertical lines guide the search for the condition of equal chemical potential in a bubble of radius ~2.5 nm (see main text for more details).

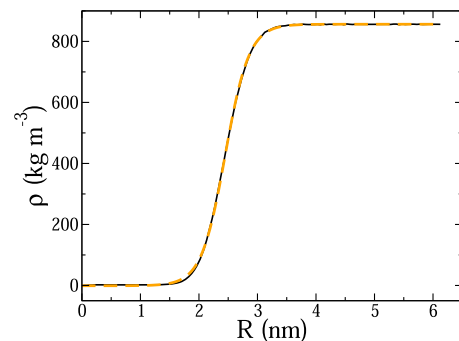


FIG. 3. Radial density profile starting from the bubble center averaged over 19 ns in the NVT ensemble (black line). The profile corresponds to a bubble surrounded by a liquid of pressure -295.4 bar. The dashed orange line is a fit to the simulation data given by Eq. (4).

where $\rho_{v,dp}$ and $\rho_{l,dp}$ are the densities of the vapor and the liquid phases obtained with the density profile (dp) fit, α is a parameter related to the width of the interfacial region, and R_{ed} is the critical bubble radius estimated as the distance at which the density is the average between both phases (“equi-density” criterion).²⁸ The equi-density radius, R_{ed} , reported in Table II is close to but systematically lower than R_G .

Both approaches obtain the radius [Eqs. (3) and (4)] assume a spherical bubble shape. In order to visually inspect the shape, we provide, in Fig. 4, a series of slabs cut through the bubble center at different times along a Seeding simulation containing a 2.5 nm bubble. The sequence of snapshots clearly shows that the bubble shape fluctuates around a sphere, which justifies our approach to obtain the bubble radius assuming an average spherical shape.

The fit parameter in Eq. (4) $\rho_{l,dp}$ is fully consistent with the density obtained by means of the overall virial pressure of the system and the bulk liquid equation of state. However, the vapor density provided by the fit given by Eq. (4), $\rho_{v,dp}$, is not accurate, given the small size of the bubbles (the sigmoid does not reach a true plateau in the interior of the bubble). Nevertheless, by estimating the vapor density as an average of the density profile in a region in the interior of the bubble, one does obtain consistent values with the vapor density resulting by imposing equal chemical potential between the bubble and the surrounding liquid. This consistency, although expected, should not be given for granted. For instance, for hard sphere crystallization, the density (and the mechanical pressure) of the crystal nucleus is lower than that obtained by imposing chemical potential homogeneity (in fact, the nucleus’s mechanical pressure is even lower than that of the surrounding liquid).^{50–52}

Knowing the bubble radius and Δp , we can use CNT to estimate the nucleation rate, J ,

$$J = A \exp\left(-\frac{\Delta G_c}{k_B T}\right), \quad (5)$$

where k_B is the Boltzmann constant, A is a kinetic pre-factor, and ΔG_c is the Gibbs free energy associated with the formation of the critical bubble, which is given by

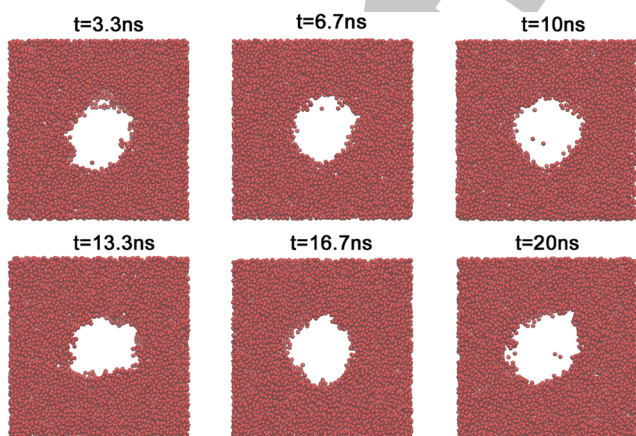


FIG. 4. Slab cuts of 20 Å thickness through the bubble center in a Seeding simulation at 450 K containing a ~2.5 nm radius sphere.

$$\Delta G_c = \frac{2\pi \times \Delta p \times R_c^3}{3}, \quad (6)$$

where R_c is the critical bubble radius that we identify either with R_G or with R_{ed} . The kinetic pre-factor is computed following Blander and Katz:²⁴

$$A = \sqrt{\frac{\Delta p \times R_c}{\pi m \rho_l}}, \quad (7)$$

where m is the mass of the molecule (18.02 u for water). This theoretical expression gives consistent results with other routes to estimate the kinetic pre-factor.⁶⁶ One can also obtain from the bubble properties an estimate of the interfacial free energy via the Laplace equation,

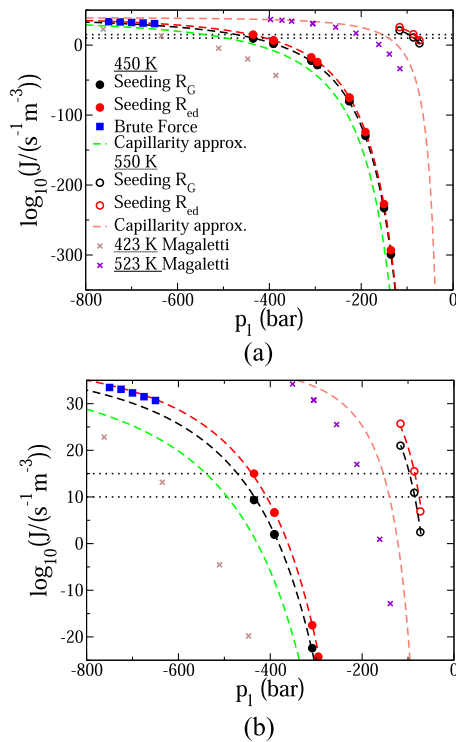
$$\gamma = \frac{\Delta p \times R_c}{2}. \quad (8)$$

In Table II, we provide the nucleation rates for all simulated bubbles alongside all parameters required for their computation. The kinetic pre-factor A can be obtained with the data reported in the table using Eq. (7) and is of the order of $10^{40} \text{ m}^{-3} \text{ s}^{-1}$ for all pressures and both choices of radius definition. The rates corresponding to R_G and R_{ed} are shown as filled black and red circles, respectively, in Fig. 5. Our data are consistent with those of Ref. 20, indicated with crosses in the figure, which were obtained with Density Functional Theory for two different temperatures, namely 423 and 523 K.

3. Surface free energy and the capillarity approximation

The surface free energy, γ , between the bubbles equilibrated in the NVT Seeding simulations and the surrounding liquid can be estimated from Eq. (8). We report them in Table II for all bubbles and plot them in Fig. 6 as a function of the liquid pressure. Again, black and red symbols correspond to the Gibbs and the equi-density definitions of the critical bubble radius, respectively. Both sets of data tend to the flat interface value (blue square) obtained from our liquid–vapor direct coexistence simulations via Eq. (1). This is a good consistency test passed by the Seeding approach. Given that γ is proportional to the bubble radius [see Eq. (8)] and that $R_{ed} < R_G$, γ coming from the equi-density radius definition is systematically lower. As one approaches coexistence (higher pressures/larger bubbles), both sets of data get closer to each other because the difference between both radii becomes a small fraction of the overall radius. The decrease of γ with pressure for the equi-density radius definition is about $1 \text{ nN m}^{-1}/100 \text{ bars pressure drop}$, whereas it is approximately half that for the Gibbs radius. In either case, γ goes down by decreasing the pressure away from coexistence. This is consistent with the results obtained in Ref. 3 at another temperature (296.4 K).

The lowering of γ by moving away from coexistence is a common feature with other systems like the Lennard–Jones fluid in the cavitation/condensation transition^{28–30,33} or ice nucleation in water.^{45,67} In our case, both the curvature of the interface and the pressure of the surrounding fluid change by moving away from coexistence. Both factors simultaneously contribute to the variation of γ , and their effects cannot be decoupled. Nevertheless, it seems intuitive that by lowering the pressure (or the density) of the liquid, the



406 **FIG. 5.** (a) Decimal logarithm of the cavitation rate as a function of the liquid pressure. Blue squares are obtained by Brute Force simulations at 450 K. Circles are
407 obtained with NVT Seeding (black circles using the Gibbs definition for the critical bubble radius [Eq. (3)] and red ones for the equi-density criterion [Eq. (4)]). Filled circles correspond to $T = 450$ K and empty ones to 550 K. The black and red
408 dashed lines are fits to the NVT Seeding data using the CNT expressions given in the main text and the $\gamma(p)$ dependence shown in Fig. 6. The green (pink) dashed
409 line represents the capillarity approximation for 450 K (550 K). The horizontal dotted lines indicate the expected rate range for cavitation in isobaric superheating¹²
410 and quartz inclusions isochoric cooling experiments.^{1,15} Crosses correspond to Density Functional Theory for 423 K (brown) and 523 K (purple).²⁰ (b) Enlargement
411 of the high nucleation rate regime.

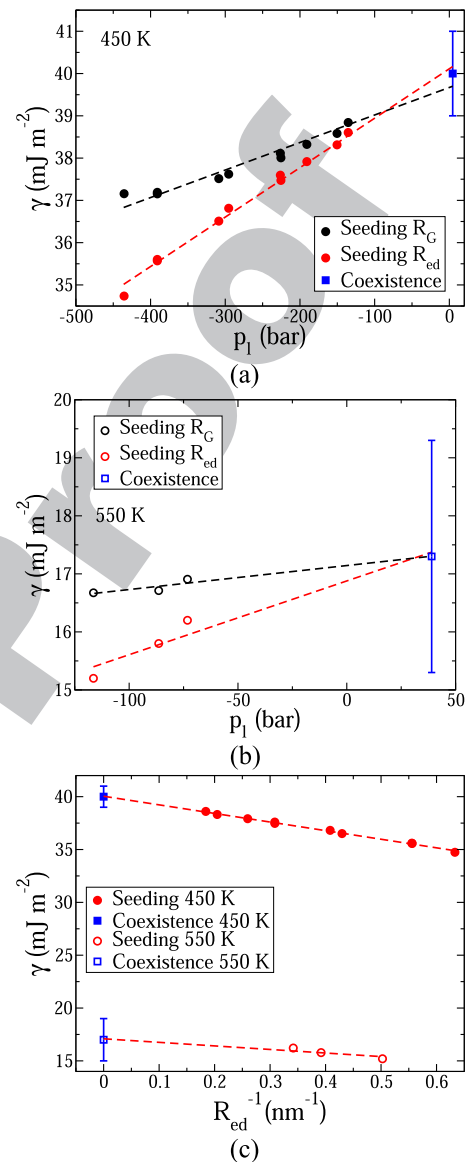
418 similarity between the vapor and the liquid increases, which is in line
419 with a γ decrease.

420 The decrease of γ with pressure looks rather linear [see
421 Fig. 6(a)]. By fitting $\gamma(p)$ to a straight line (dashed in Fig. 6) and
422 using Eqs. (5)–(8), we can fit the rate-pressure dependence²⁹ and
423 obtain the dashed curves in Fig. 5, which we comment on in more
424 detail in Sec. III B 4.

425 The variation of γ with curvature is often described by the
426 following expression proposed by Tolman:⁶⁵

$$427 \quad \gamma = \gamma_c \left(1 - \frac{2\delta}{R_c} \right), \quad (9)$$

428 where δ is the Tolman length, which can be obtained from the slope
429 of a γ vs $1/R_c$ representation such as that shown in Fig. 6(c) (filled
430 data correspond to 450 K). We use $R_c = R_{ed}$ to do such representation
431 given that, as it will be shown later on, it turns out that R_{ed} better
432 predicts the nucleation rate in the spontaneous cavitation regime. A
433 positive δ is expected, given that γ diminishes as curvature increases.



434 **FIG. 6.** (a) and (b) Interfacial free energy as a function of the liquid pressure. Black and red symbols correspond to estimates of γ from the NVT Seeding
435 simulations using Eqs. (3) and (4) to obtain the bubble radius, respectively. The blue square corresponds to the coexistence value obtained with simulations of
436 a flat vapor–liquid interface via Eq. (1). (a) and (b) correspond to 450 and 550 K, respectively. (c) Interfacial free energy vs the inverse equi-density radius for both
437 temperatures as indicated in the legend. 438 439 440

441 The resulting δ is 0.1 nm. Later on, in Sec. III B 5, we extend our
442 study to a temperature of 550 K in order to compare our simu-
443 lations with experiments. Here, we anticipate the results for this
444 temperature regarding the Tolman length. From the representation
445 in Fig. 6(c) (empty symbols), we get the same δ as for 450 K, 0.1 nm,
446 suggesting that δ is temperature independent. A very recent simu-
447 lation estimate of δ at $T = 296.4$ K (0.091 ± 0.008 nm) using the same

448 model as in this work confirms the non-dependence of the Tolman
449 length with temperature.

450 Taking into account, the decrease of γ when lowering the liquid
451 pressure is crucial to get accurate estimates of the nucleation rate. To
452 illustrate this, we compute the rate that would be obtained by con-
453 sidering γ constant and equal to its value at coexistence (capillarity
454 approximation). To obtain such a rate, we express Eqs. (7) and (6) as
455 a function of γ via Eq. (8). Thus, one gets

$$456 \quad \Delta G_c = \frac{16\pi\gamma^3}{3\Delta p^2}, \quad (10)$$

and

$$457 \quad A = \rho_l \sqrt{\frac{2\gamma}{\pi m}}. \quad (11)$$

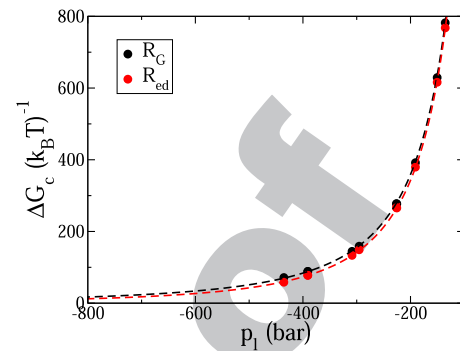
458 Inserting Eqs. (11) and (10) into Eq. (5) and using the coexistence
459 γ for every pressure gives rise to the green dashed curve in Fig. 5,
460 which lies at lower rates as compared to Seeding or Brute Force data.
461 The capillarity approximation actually underestimates J by 6 orders
462 of magnitude when compared to Brute Force. The conclusion is that
463 a theoretical or a simulation treatment (Seeding and Brute Force in
464 the present case) that takes into consideration the variation of γ with
465 pressure/curvature is indeed needed to obtain accurate cavitation
466 rates in overstretched water, not enough the use of the capillarity
467 approximation. It was also concluded that the capillarity approxima-
468 tion fails to provide accurate nucleation rates for water cavitation, in
469 previous simulations and theoretical studies.^{2,3,20}

4. Cavitation rate: Brute force vs Seeding

471 In Fig. 5 we plot the rate vs the liquid pressure as obtained from
472 Brute Force simulations (blue squares) and Seeding (black and red
473 circles using R_G and R_{ed} as definitions for the critical radius, respec-
474 tively). More than 300 orders of magnitude of the nucleation rate
475 are spanned by our data. Brute Force data cover the highly negative
476 pressure regime, where cavitation is spontaneous in the simulation
477 time, whereas Seeding is used to obtain rate estimates in a higher
478 pressure regime, where the rate is much lower and nucleation does
479 not spontaneously occur. As discussed later on, the Seeding regime
480 is more relevant to experiments.

481 The Gibbs radius systematically gives smaller rates than the
482 equi-density one (by about 4–5 orders of magnitude), given that
483 the nucleation barrier is proportional to the cubed bubble radius
484 [Eq. (6)] and $R_G > R_{ed}$. An extrapolation to low pressures of the fits
485 to Seeding data [done by linearly extrapolating the $\gamma(p)$ fits shown
486 in Fig. 6(a)] suggests that by using R_{ed} as radius definition, a bet-
487 ter consistency with Brute Force is achieved [see the enlargement
488 shown in Fig. 5(b)]. We stress that the Brute Force rate is exempt
489 from theoretical approximations. In this respect, R_{ed} seems to be a
490 better definition than R_G of the critical bubble radius, R_c , in the CNT
491 expressions given by Eqs. (6)–(8).

492 In Fig. 7, we plot the Gibbs free energy barrier, ΔG_c , com-
493 puted according to Eq. (6), from our Seeding simulations (dots)
494 fitted via the linear $\gamma(p)$ dependence found in Fig. 6. The predicted
495 free energy barrier height in the spontaneous cavitation pressure
496 range (–750 to –650 bars) goes from 15 to 20 $k_B T$ according to
497 the R_{ed} radius definition. These barrier heights are typical of sponta-
498 neous nucleation events in simulations.^{50,68} This consistency further



499 **FIG. 7.** Gibbs free energy as a function of the liquid pressure from Seeding sim-
500 ulations considering the equi-density radius definition. 450 K. Black (red) circles are
501 data obtained using the Gibbs (equi-density) radius definition. Dashed curves are
502 fits based on the linear $\gamma(p)$ dependence shown in Fig. 6.

503 demonstrates the match between Brute Force and Seeding extrapo-
504 lated via the $\gamma(p)$ linear dependence of the data obtained with the
505 equi-density radius definition.

5. Comparison with experiments

506 Experimental studies of cavitation, rather than having direct
507 access to the nucleation rate, detect the thermodynamic state point at
508 which a liquid water sample undergoes cavitation. In Fig. 8, the cavi-
509 tation pressure is plotted against temperature. Empty and solid sym-
510 bols correspond to experimental measurements and simulations,
511 respectively. Lines correspond to theoretical predictions.

512 We compare first our data against experiments of isobaric
513 superheating¹² and isochoric cooling, the latter performed with
514 quartz inclusions.^{1,15} The cavitation rate probed in these exper-
515 iments, J_{exp} , is determined by the product of the employed
516 volumes and observation times and ranges from 10^{10} to 10^{15}
517 ($m^{-3} s^{-1}$).^{1,15,19,69} Therefore, in order to compare our simulations
518 against experiments, we have to find the pressure range that gives
519 the aforementioned rates (indicated with dotted horizontal lines
520 in Fig. 5). By using this strategy of identifying iso-rate lines and
521 with simulations, we were able to satisfactorily predict the location
522 of the so-called homogeneous ice nucleation line in studies of ice
523 nucleation.⁷⁰

524 Using the $J(p)$ curves in Fig. 5, we can estimate by interpola-
525 tion that cavitation in the experiments mentioned in the previous
526 paragraph will occur between $p(J = 10^{10} m^{-3} s^{-1}) = -41$ MPa and
527 $p(J = 10^{15} m^{-3} s^{-1}) = -44$ MPa at 450 K (we used the R_{ed} radius
528 definition for this estimate, but the values obtained using R_G are very
529 similar). This pressure range is quite narrow due to the large slope
530 of the $J(p)$ curve. Such pressure range is our simulation estimate
531 for the occurrence of cavitation in experiments of isobaric super-
532 heating or isochoric cooling (in quartz inclusions) at 450 K and is
533 indicated with a red dot for R_{ed} and with a black dot for R_G in Fig. 8
534 [the size of the dot includes the values of $p(J = 10^{10} - 10^{15} m^{-3} s^{-1})$].
535 It is worth pointing out that at the pressures where we predict cavi-
536 tation to occur in experiments (–41 to –44 MPa), we obtain a ΔG_c of
537 60–70 $k_B T$ from the fit to the R_{ed} data shown in Fig. 7. These barrier
538 heights are typical of nucleation experiments.
539

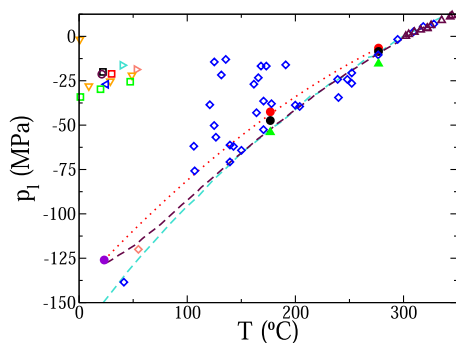


FIG. 8. Cavitation pressure as a function of temperature obtained with experiments (empty symbols), simulations (filled symbols), and theory (dashed lines). Black and red filled dots correspond to our Seeding simulation predictions using R_G and R_{ed} as the radius definition, respectively, whereas the purple dot corresponds to transition sampling simulations.³ The dotted line is a spline fit to simulation data to help visualize the trend predicted by TIP4P/2005. Filled green up triangles are predictions combining simulation equations of state with the capillarity approximation (see main text). The cyan dashed line is a CNT-like prediction from Refs. 1 and 25 and the maroon one is a density functional approach.²⁰ Blue¹ and pink¹⁵ empty diamonds correspond to the inclusion of isochoric cooling experiments. Empty maroon up triangles are data from isobaric superheating experiments.¹² Right triangles correspond to Berthelot isochoric cooling experiments, in pale blue¹⁶ and in pink.¹⁷ Centrifuge experiments are represented with orange down triangles,⁷² shock wave experiments with blue up triangles,⁷³ and acoustic experiments with squares, in black from Ref. 14, in red from Ref. 37, and in green from Ref. 38. The maroon circle is obtained using artificial trees.¹⁸

The dot in Fig. 8 obtained from our simulations at 450 K lies in the low pressure limit of the rather scattered experimental data cloud (blue empty diamonds) found around 450 K. This is consistent with the hypothesis that, around this temperature, there might be heterogeneous cavitation in the experiments,¹ which is a pathway that leads to bubble nucleation at higher pressures than its homogeneous counterpart. Our simulation point, obviously, corresponds to homogeneous nucleation, which is why it stands close to the lowest attainable experimental pressures.

At high temperatures, the experimental data are not scattered anymore, and they all nicely fall into a neat line. In order to compare our simulations with experiments in such a temperature regime, we performed extra *NVT* Seeding simulations at 550 K. The simulation details are identical to those described for 450 K except that we used a lower integration time step, namely 1 fs. At 550 K, we find a coexistence pressure of 39(1) bars and an interfacial free energy of 17(2) mJ m⁻², both consistent with Ref. 61 (38.01 bars) and Ref. 62 (38.3 bars and 17.4 mJ m⁻²).

We run first a bubble of radius about 3 nm. We observe that the interfacial width at 550 K doubles that of 450 K (2 vs 1 nm). In equilibrium at 550 K, the bubble is surrounded by a liquid of $p = -73.2$ bars. Since its corresponding rate, $J = 10^7$ m⁻³ s⁻¹ (with the R_{ed} radius criterion), turned out to lie below the J range relevant to experiments, 10^{10} – 10^{15} m⁻³ s⁻¹, we decided to equilibrate a couple of smaller bubbles in order to enable the interpolation. The rates calculated from the three Seeding runs are reported in Table II and are represented as empty circles in Fig. 5 [the kinetic pre-factor, which can be obtained with the data of the table using Eq. (7), is of the same order of magnitude as that found at 450 K: 10^{40} m⁻³ s⁻¹]. The $\gamma(p)$

dependence shown in Fig. 6(b) is used to fit the $J(p)$ data at 550 K (dashed lines through empty circles in Fig. 5). By interpolation, we estimate that cavitation at 550 K will take place between -7.6 and -8.5 MPa (using the R_{ed} radius definition). This pressure interval is included as a red dot in Fig. 8 and is quite close to the experimental line, which highlights the ability of the TIP4P/2005 model, in combination with the Seeding technique, to predict and justify the experimental cavitation behavior. In Fig. 8, we also include two low temperature data coming from inclusion experiments (pink empty diamond¹⁵) and simulations (purple solid circle³). Again, simulations and inclusion experiments seem to be fully consistent with each other.

To summarize, our simulations seem to be in good agreement with superheating¹² and with quartz inclusion experiments¹ at high temperatures, and those of Ref. 3 are consistent with more recent quartz inclusions experiments performed at lower temperatures.¹⁵ We include in Fig. 8 a spline fit (red dotted line) to the three available simulation data (450 and 550 K from this work and 296.4 K from Ref. 3) to give a visual idea of the cavitation line predicted by the TIP4P/2005 model. A direct comparison between the model and the experiment is enabled by the fact that TIP4P/2005 predicts quite well the critical temperature and the vapor pressure.⁶¹ The model seems to mildly overestimate the cavitation pressure, which indicates that TIP4P/2005 overestimates the nucleation rate. Such overestimation could be due to the model having a smaller γ than real water.⁶² Also, it should be taken into account that γ is very sensitive to the employed cutoff and that using larger cutoff distances could improve the agreement between simulation and experiment.^{62,71} In any case, the model predictions shown in Fig. 8 are already very satisfactory.

However, the scenario is not fully clear yet: measurements of the cavitation pressure with other strategies, such as the Berthelot, centrifuge, acoustic cavitation, and artificial tree techniques, indicated with empty symbols of different colors forming a cloud located at around -25 MPa and between 0 and 25 °C, do not agree with the trend set by our simulations and those of Ref. 3. All these experiments find cavitation pressures well above those predicted by the simulations. In acoustic cavitation experiments, according to Ref. 35, the accessible rate is of the order of 10^{20} m⁻³ s⁻¹. This is 5 orders of magnitude higher than the highest value we have used in this paper (and in Ref. 3) to compare with inclusion experiments. However, if we had used the 10^{20} m⁻³ s⁻¹ rate, we would have found an even larger discrepancy because we would have predicted a lower cavitation pressure (pressure goes down as the rate goes up). Hence, we are unable to explain the discrepancy with acoustic cavitation experiments. What about Berthelot's experiments? In such experiments, isochoric cooling is performed as in quartz inclusions but in much larger volumes (about 5 orders of magnitude larger, 10^{-10} vs 10^{-15} m³).¹⁶ Also, the observation time is longer in Berthelot experiments (10^4 vs 10 s). With these time and volume scales, rates as low as 10^5 m⁻³ s⁻¹ could be probed in Berthelot experiments. Inferring the cavitation pressure from $J = 10^5$ m⁻³ s⁻¹, which is 5 orders of magnitude below the lower rate bound here considered, would go in the right direction, although it is not enough: both in our work at 450 K and in that of Ref. 3 at 296.4 K, one can see that, in the experimentally relevant region (that given by the dotted lines in Fig. 5), the pressure barely changes 3 MPa every 5 orders of magnitude change of the rate. This is clearly insufficient to explain the ~ 100 MPa

643 difference between simulations and Berthelot experiments shown in
644 Fig. 8. Possibly, the explanation for such a large discrepancy between
645 simulations and Berthelot or other sorts of experiments is that cavi-
646 tation occurs at large pressures via heterogeneous nucleation in these
647 experiments.

648 Finally, in Fig. 8, we also include the capillarity approxima-
649 tion prediction for the cavitation pressure in isobaric superheating
650 or quartz inclusion experiments (green upward triangles). These tri-
651 angles lie at lower pressures than circles corresponding to Seeding
652 predictions. This is justified as follows: We have already discussed
653 in Fig. 5 that the rate obtained from the capillarity approxima-
654 tion is lower than that coming from Seeding due to the decrease
655 of γ as the bubble radius diminishes (see Fig. 6). Since the cap-
656 ilarity rate is lower, the pressure at which capillarity predicts a
657 certain rate is lower too. However, it is perhaps surprising that the
658 capillarity approximation prediction for the cavitation pressure is
659 quite close to that obtained by Seeding despite the fact that capil-
660 larity rates lie 5–10 orders of magnitude below Seeding (see Fig. 5).
661 Again, this is explained by the steep $J(p)$ curve in the experimen-
662 tally relevant region (large rate changes correspond to rather small
663 pressure variations). This justifies the proximity between Seeding
664 and capillarity predictions of the cavitation pressure and between
665 different theoretical approaches shown in Fig. 8, disregarding^{1,25} or
666 taking into account²⁰ the variation of the interfacial free energy with
667 pressure.

668 IV. SUMMARY AND CONCLUSIONS

669 We investigate water cavitation with molecular dynamics simu-
670 lations using the TIP4P/2005 model. Our first goal is to establish
671 the cavitation rate vs pressure curve at 450 K. For that purpose, we
672 first evaluate the coexistence properties by simulating the liquid in
673 contact with the vapor phase in direct coexistence. We find that the
674 coexistence pressure is 4.49 bars and that the interfacial free energy is
675 $40(1) \text{ mJ m}^{-2}$. We then simulate the liquid at large negative pressures
676 until we find a regime where vapor bubbles spontaneously form in
677 the course of an unbiased simulation. Due to the small size of the
678 simulation volumes as compared to experimental ones, this regime
679 is found at very low pressures: below -650 bar. In such simulations,
680 we can estimate the nucleation rate by computing the average time
681 required for a bubble to appear in the simulated liquid volume. We
682 find nucleation rates in the range of 10^{30} – $10^{33} \text{ m}^{-3} \text{ s}^{-1}$ when lower-
683 ing the pressure from -650 to -750 bar. We cannot simulate lower
684 pressures because there is no longer an induction period before the
685 appearance of a bubble. To compute the nucleation rate at larger
686 pressures, which are more relevant to experiments, we resort to the
687 Seeding method, which consists in simulating a bubble surrounded
688 by the liquid in the *NVT* ensemble, in our case at 450 K. In such sim-
689 ulations, we compute the average pressure of the surrounding liquid
690 with the virial expression and the bubble radius by means of radial
691 density profiles (equi-density criterion). Alternatively, the radius is
692 estimated using the definition of the equi-molar Gibbs dividing sur-
693 face, which only requires knowing the volume of the simulation box,
694 the total number of molecules, the liquid density, and the vapor
695 density. To obtain the latter, we use thermodynamic integration
696 of the equation of state of both phases, previously obtained with
697 bulk phase simulations, and impose the condition of homogeneous
698 chemical potential throughout the system. The vapor density thus

699 obtained is consistent with that inferred from the density profile.
700 This is expected in vapor–liquid transitions but is not generally true
701 in solid–liquid equilibrium.^{51,52} We combine the aforementioned
702 simulation information (pressure of both phases, and bubble radius)
703 with CNT to obtain estimates of the nucleation rate and the interfa-
704 cial free energy. We get a huge variation of the nucleation rate (from
705 10^{-300} to $10^{10} \text{ m}^{-3} \text{ s}^{-1}$) in the pressure range going from -130 to
706 -430 bar. The interfacial free energy goes down from its coexistence
707 value as pressure goes down. The Gibbs radius definition predicts
708 an interfacial free energy drop of $\sim 0.5 \text{ mN/m/100 bars}$ decrease
709 whereas the equi-density definition predicts approximately double
710 that. Both criteria to identify the bubble radius give a similar rate
711 trend although the Gibbs criterion gives lower values because it
712 predicts higher interfacial free energies. By fitting the variation of
713 the interfacial free energy with pressure to a straight line, we can
714 fit the rate data obtained with Seeding. We find that the fit to the
715 Seeding data obtained with the equi-density radius definition extrap-
716 olates better to the regime where we computed the nucleation rate
717 with unbiased simulations. Thus, the equi-density radius seems to
718 be more appropriate to describe water cavitation with CNT. The γ
719 variation with curvature obtained with the equi-density radius is fit-
720 ted by a 0.1 nm Tolman length. We also compare the Seeding rate
721 curves with those obtained using the capillarity approximation, i.e.,
722 by assuming that the interfacial free energy does not vary with pres-
723 sure. Obviously, the capillarity curve predicts lower rates because
724 it does not take into consideration the lowering of the interfacial
725 free energy when moving away from coexistence. Finally, we com-
726 pare our results with experiments. The experimental data available
727 at 450 K are rather scattered so we decided to run a few extra Seeding
728 simulations at 550 K where there are cleaner data. To compare with
729 experiments, we need to predict the pressure at which the system
730 undergoes cavitation at a given temperature. We do this prediction
731 by interpolating, in our rate vs pressure curves, the rate at which it
732 is expected that cavitation takes place in the experiments. With this
733 strategy, we get a successful comparison with both isobaric heat-
734 ing and isochoric cooling experiments with small volumes (quartz
735 inclusions). However, we find irreconcilable discrepancies with the
736 cavitation pressures obtained with other experimental techniques
737 like Berthelot or acoustic cavitation. We hypothesize that there could
738 be heterogeneous bubble nucleation in such experiments, given that
739 cavitation occurs at much higher pressures than predicted by our
740 simulations and those of Ref. 3, performed at 296.4 K. Overall,
741 our work shows an efficient manner to investigate and understand
742 the factors that control and affect water cavitation using molecular
743 simulations.

744 ACKNOWLEDGMENTS

745 This project has been funded by the Ministry of Science
746 and Innovation under Grant No. PID2019-105898GB-C21. E.G.N.
747 thanks Agencia Estatal de Investigación and Fondo Europeo
748 de Desarrollo Regional (FEDER) under Grant No. PID2020-
749 115722GB-C21. C.P.L. thanks Ministerio de Universidades for a
750 predoctoral Formación Profesorado Universitario under Grant No.
751 FPU18/03326 and also Ayuntamiento de Madrid for a Residen-
752 cia de Estudiantes grant. The authors acknowledge the computer
753 resources and technical assistance provided by the Red Española de
754 Supercomputación (RES).

755 **AUTHOR DECLARATIONS**756 **Conflict of Interest**

757 The authors have no conflicts to disclose.

758 **Author Contributions**

759 **Cintia P. Lamas:** Conceptualization (equal); Data curation (equal);
760 Formal analysis (equal); Investigation (equal); Methodology (equal);
761 Writing – original draft (supporting); Writing – review & editing
762 (equal). **Carlos Vega:** Conceptualization (equal); Funding acquisition
763 (equal); Project administration (equal); Supervision (equal);
764 Writing – review & editing (equal). **Eva G. Noya:** Conceptualization
765 (equal); Data curation (equal); Project administration (equal);
766 Resources (equal); Supervision (equal); Validation (equal); Writing
767 – review & editing (equal). **Eduardo Sanz:** Conceptualization
768 (equal); Data curation (equal); Funding acquisition (equal); Method-
769 ology (equal); Project administration (equal); Supervision (equal);
770 Writing – original draft (equal); Writing – review & editing (equal).

771 **DATA AVAILABILITY**772 The data that support the findings of this study are available
773 within the article.774 **REFERENCES**

- 775 ¹Q. Zheng, D. J. Durben, G. H. Wolf, and C. A. Angell, “Liquids at large nega-
776 tive pressures: Water at the homogeneous nucleation limit,” *Science* **254**, 829–832
(1991).
777 ²F. Caupin, “Liquid-vapor interface, cavitation, and the phase diagram of water,”
778 *Phys. Rev. E* **71**, 051605 (2005).
779 ³G. Menzl, M. A. Gonzalez, P. Geiger, F. Caupin, J. L. F. Abascal, C. Valeriani, and
780 C. Dellago, “Molecular mechanism for cavitation in water under tension,” *Proc.*
781 *Natl. Acad. Sci. U. S. A.* **113**, 13582–13587 (2016).
782 ⁴P. G. Debenedetti and H. E. Stanley, “Supercooled and glassy water,” *Phys. Today*
783 **56**, 40 (2003).
784 ⁵M. Shusser and D. Weihs, “Explosive boiling of a liquid droplet,”
785 *Int. J. Multiphase Flow* **25**, 1561–1573 (1999).
786 ⁶M. Shusser, T. Ytrehus, and D. Weihs, “Kinetic theory analysis of explosive
787 boiling of a liquid droplet,” *Fluid Dyn. Res.* **27**, 353 (2000).
788 ⁷A. Toramaru, “Vesiculation process and bubble size distributions in ascending
789 magmas with constant velocities,” *J. Geophys. Res.: Solid Earth* **94**, 17523–17542,
790 <https://doi.org/10.1029/jb094ib12p17523> (1989).
791 ⁸H. Massol and T. Koyaguchi, “The effect of magma flow on nucleation of gas
792 bubbles in a volcanic conduit,” *J. Volcanol. Geotherm. Res.* **143**, 69–88 (2005).
793 ⁹C. E. Brennen, *Cavitation and Bubble Dynamics* (Cambridge University Press,
2014).
794 ¹⁰K. S. Suslick, “Sonochemistry,” *Science* **247**, 1439–1445 (1990).
795 ¹¹K. S. Suslick, M. M. Mdeleleni, and J. T. Ries, “Chemistry induced by
796 hydrodynamic cavitation,” *J. Am. Chem. Soc.* **119**, 9303–9304 (1997).
797 ¹²V. Skripov, in *Water and Steam*, edited by J. Straub and K. Scheffler (Pergamon,
798 Elmsford, 1980).
799 ¹³E. Herbert, S. Balibar, and F. Caupin, “Cavitation pressure in water,”
800 *Phys. Rev. E* **74**, 041603 (2006).
801 ¹⁴W. J. Galloway, “An experimental study of acoustically induced cavitation in
802 liquids,” *J. Acoust. Soc. Am.* **26**, 849–857 (1954).
803 ¹⁵M. E. M. Azouzi, C. Ramboz, J.-F. Lenain, and F. Caupin, “A coherent picture
804 of water at extreme negative pressure,” *Nat. Phys.* **9**, 38–41 (2013).
805 ¹⁶S. J. Henderson and R. J. Speedy, “A Berthelot-Bourdon tube method for
806 studying water under tension,” *J. Phys. E: Sci. Instrum.* **13**, 778 (1980).

- ¹⁷K. Hiro, Y. Ohde, and Y. Tanzawa, “Stagnations of increasing trends in nega-
807 tive pressure with repeated cavitation in water/metal Berthelot tubes as a result of
808 mechanical sealing,” *J. Phys. D: Appl. Phys.* **36**, 592 (2003).
809 ¹⁸T. D. Wheeler and A. D. Stroock, “The transpiration of water at negative
810 pressures in a synthetic tree,” *Nature* **455**, 208–212 (2008).
811 ¹⁹F. Caupin and E. Herbert, “Cavitation in water: A review,” *C. R. Phys.* **7**,
812 1000–1017 (2006).
813 ²⁰F. Magaletti, M. Gallo, and C. M. Casciola, “Water cavitation from ambient to
814 high temperatures,” *Sci. Rep.* **11**, 20801 (2021).
815 ²¹H. Kanno, R. J. Speedy, and C. A. Angell, “Supercooling of water to -92°C
816 under pressure,” *Science* **189**, 880–881 (1975).
817 ²²P. G. Debenedetti, *Metastable Liquids: Concepts and Principles* (Princeton
818 University Press, 1996).
819 ²³K. F. Kelton, *Crystal Nucleation in Liquids and Glasses* (Academic, Boston,
820 1991).
821 ²⁴M. Blander, and J. L. Katz., “Bubble nucleation in liquids,” *AIChE J.* **21**, 833–848
(1975).
822 ²⁵J. C. Fisher, “The fracture of liquids,” *J. Appl. Phys.* **19**, 1062–1067 (1948).
823 ²⁶Z.-J. Wang, C. Valeriani, and D. Frenkel, “Homogeneous bubble nucleation
824 driven by local hot spots: A molecular dynamics study,” *J. Phys. Chem. B* **113**,
825 3776–3784 (2008).
826 ²⁷S. L. Meadley and F. A. Escobedo, “Thermodynamics and kinetics of bubble
827 nucleation: Simulation methodology,” *J. Chem. Phys.* **137**, 074109 (2012).
828 ²⁸P. Rosales-Pelaez, M. I. Garcia-Cid, C. Valeriani, C. Vega, and E. Sanz, “Seeding
829 approach to bubble nucleation in superheated Lennard-Jones fluids,” *Phys. Rev. E*
830 **100**, 052609 (2019).
831 ²⁹P. Rosales-Pelaez, I. Sanchez-Burgos, C. Valeriani, C. Vega, and E. Sanz,
832 “Seeding approach to nucleation in the NVT ensemble: The case of bubble
833 cavitation in overstretched Lennard Jones fluids,” *Phys. Rev. E* **101**, 022611 (2020).
834 ³⁰I. Sanchez-Burgos, P. M. de Hijes, P. Rosales-Pelaez, C. Vega, and E. Sanz,
835 “Equivalence between condensation and boiling in a Lennard-Jones fluid,” *Phys.*
836 *Rev. E* **102**, 062609 (2020).
837 ³¹S. Marchio, S. Meloni, A. Giacomello, C. Valeriani, and C. M. Casciola,
838 “Pressure control in interfacial systems: Atomistic simulations of vapor
839 nucleation,” *J. Chem. Phys.* **148**, 064706 (2018).
840 ³²V. G. Baidakov and K. R. Protchenko, “Molecular dynamics simulation of cavi-
841 tation in a Lennard-Jones liquid at negative pressures,” *Chem. Phys. Lett.* **760**,
842 138030 (2020).
843 ³³C. P. Lamas, E. Sanz, C. Vega, and E. G. Noya, “Estimation of bubble cavi-
844 tation rates in a symmetrical Lennard-Jones mixture by NVT Seeding simulations,”
845 *J. Chem. Phys.* (submitted) (2023).
846 ³⁴J. L. F. Abascal and C. Vega, “A general purpose model for the condensed phases
847 of water: TIP4P/2005,” *J. Chem. Phys.* **123**, 234505 (2005).
848 ³⁵F. Caupin, A. Arvengas, K. Davitt, M. E. M. Azouzi, K. I. Shmulovich,
849 C. Ramboz, D. A. Sessoms, and A. D. Stroock, “Exploring water and other liquids
850 at negative pressure,” *J. Phys.: Condens. Matter* **24**, 284110 (2012).
851 ³⁶K. Davitt, A. Arvengas, and F. Caupin, “Water at the cavitation limit: Density
852 of the metastable liquid and size of the critical bubble,” *Europhys. Lett.* **90**, 16002
853 (2010).
854 ³⁷M. Greenspan and C. E. Tschiegg, “Radiation-induced acoustic cavitation;
855 apparatus and some results,” *J. Res. Natl. Bur. Stand., Sect. C* **71**, 299 (1967).
856 ³⁸K. Davitt, A. Arvengas, and F. Caupin, “Water at the cavitation limit: Density
857 of the metastable liquid and size of the critical bubble,” *Europhys. Lett.* **90**, 16002
858 (2010).
859 ³⁹L. G. MacDowell, V. K. Shen, and J. R. Errington, “Nucleation and cavitation of
860 spherical, cylindrical, and slablike droplets and bubbles in small systems,” *J. Chem.*
861 *Phys.* **125**, 034705 (2006).
862 ⁴⁰M. Schrader, P. Virnau, and K. Binder, “Simulation of vapor-liquid coexistence
863 in finite volumes: A method to compute the surface free energy of droplets,” *Phys.*
864 *Rev. E* **79**, 061104 (2009).
865 ⁴¹K. Binder, B. J. Block, P. Virnau, and A. Tröster, “Beyond the van der Waals
866 loop: What can be learned from simulating Lennard-Jones fluids inside the region
867 of phase coexistence,” *Am. J. Phys.* **80**, 1099–1109 (2012).
868 ⁴²X.-M. Bai and M. Li, “Calculation of solid-liquid interfacial free energy: A
869 classical nucleation theory based approach,” *J. Chem. Phys.* **124**, 124707 (2006).
870

- 868 ⁴³R. G. Pereyra, I. Szleifer, and M. A. Carignano, "Temperature dependence of ice
869 critical nucleus size," *J. Chem. Phys.* **135**, 034508 (2011).
- 870 ⁴⁴B. C. Knott, V. Molinero, M. F. Doherty, and B. Peters, "Homogeneous nucle-
871 ation of methane hydrates: Unrealistic under realistic conditions," *J. Am. Chem.*
872 *Soc.* **134**, 19544–19547 (2012).
- 873 ⁴⁵E. Sanz, C. Vega, J. R. Espinosa, R. Caballero-Bernal, J. L. F. Abascal, and
874 C. Valeriani, "Homogeneous ice nucleation at moderate supercooling from
875 molecular simulation," *J. Am. Chem. Soc.* **135**, 15008–15017 (2013).
- 876 ⁴⁶J. R. Espinosa, C. Vega, C. Valeriani, and E. Sanz, "Seeding approach to crystal
877 nucleation," *J. Chem. Phys.* **144**, 034501 (2016).
- 878 ⁴⁷R. Becker and W. Döring, "Kinetische behandlung der keimbildung in
879 übersättigten dampfen," *Ann. Phys.* **416**, 719–752 (1935).
- 880 ⁴⁸J. W. Gibbs, "On the equilibrium of heterogeneous substances," *Trans. Connect.*
881 *Acad. Sci.* **3**, 108–248 (1876).
- 882 ⁴⁹J. W. Gibbs, "On the equilibrium of heterogeneous substances," *Trans. Connect.*
883 *Acad. Sci.* **16**, 343–524 (1878).
- 884 ⁵⁰P. Montero de Hijes, J. R. Espinosa, E. Sanz, and C. Vega, "Interfacial free energy
885 of a liquid-solid interface: Its change with curvature," *J. Chem. Phys.* **151**, 144501
(2019).
- 886 ⁵¹P. Montero de Hijes, J. R. Espinosa, V. Bianco, E. Sanz, and C. Vega, "Interfacial
887 free energy and Tolman length of curved liquid–solid interfaces from equilibrium
888 studies," *J. Phys. Chem. C* **124**, 8795–8805 (2020).
- 889 ⁵²P. Montero de Hijes, K. Shi, E. G. Noya, E. E. Santiso, K. E. Gubbins, E. Sanz,
890 and C. Vega, "The Young–Laplace equation for a solid–liquid interface," *J. Chem.*
891 *Phys.* **153**, 191102 (2020).
- 892 ⁵³B. Hess, C. Kutzner, D. van der Spoel, and E. Lindahl, "Algorithms for highly
893 efficient, load-balanced, and scalable molecular simulation," *J. Chem. Theory*
894 *Comput.* **4**, 435–447 (2008).
- 895 ⁵⁴M. Parrinello and A. Rahman, "Polymorphic transitions in single crystals: A
896 new molecular dynamics method," *J. Appl. Phys.* **52**, 7182 (1981).
- 897 ⁵⁵G. J. Martyna, M. L. Klein, and M. Tuckerman, "Nosé–Hoover chains: The
898 canonical ensemble via continuous dynamics," *J. Chem. Phys.* **97**, 2635–2643
(1992).
- 899 ⁵⁶D. R. Wheeler and J. Newman, "A less expensive Ewald lattice sum," *Chem.*
900 *Phys. Lett.* **366**, 537 (2002).
- 901 ⁵⁷S. E. Feller, R. W. Pastor, A. Rojnuckarin, S. Bogusz, and B. R. Brooks, "Effect
902 of electrostatic force truncation on interfacial and transport properties of water,"
903 *J. Phys. Chem.* **100**, 17011–17020 (1996).
- 904 ⁵⁸I. Sanchez-Burgos, M. C. Muniz, J. R. Espinosa, and A. Z. Panagiotopoulos, "A
905 deep potential model for liquid-vapor equilibrium and cavitation rates of water,"
906 *arXiv:2301.12008* (2023).
- 907 ⁵⁹B. Hess, H. Bekker, H. J. C. Berendsen, and J. G. E. M. Fraaije, "LINCS: A linear
908 constraint solver for molecular simulations," *J. Comput. Chem.* **18**, 1463–1472
(1997).
- 909 ⁶⁰B. Hess, "P-LINCS: A parallel linear constraint solver for molecular simulation,"
910 *J. Chem. Theory Comput.* **4**, 116–122 (2008).
- 911 ⁶¹C. Vega, J. L. F. Abascal, and I. Nezbeda, "Vapor-liquid equilibria from
912 the triple point up to the critical point for the new generation of TIP4P-like
913 models: TIP4P/Ew, TIP4P/2005, and TIP4P/ice," *J. Chem. Phys.* **125**, 034503
(2006).
- 914 ⁶²C. Vega and E. de Miguel, "Surface tension of the most popular models of water
915 by using the test-area simulation method," *J. Chem. Phys.* **126**, 154707 (2007).
- 916 ⁶³J. S. Rowlinson and B. Widom, *Molecular Theory of Capillarity* (Courier
917 Corporation, 2013).
- 918 ⁶⁴J. Gibbs, *The collected works*, Vol. I, 1928.
- 919 ⁶⁵R. C. Tolman, "The effect of droplet size on surface tension," *J. Chem. Phys.* **17**,
920 333–337 (1949).
- 921 ⁶⁶I. S. Joung and T. E. Cheatham, "Determination of alkali and halide monovalent
922 ion parameters for use in explicitly solvated biomolecular simulations," *J. Phys.*
923 *Chem. B* **112**, 9020–9041 (2008).
- 924 ⁶⁷J. R. Espinosa, E. Sanz, C. Valeriani, and C. Vega, "Homogeneous ice
925 nucleation evaluated for several water models," *J. Chem. Phys.* **141**, 18C529
(2014).
- 926 ⁶⁸L. Filion, M. Hermes, R. Ni, and M. Dijkstra, "Crystal nucleation of hard
927 spheres using molecular dynamics, umbrella sampling, and forward flux sam-
928 pling: A comparison of simulation techniques," *J. Chem. Phys.* **133**, 244115
(2010).
- 929 ⁶⁹P. V. Skripov and A. P. Skripov, "The phenomenon of superheat of liq-
930 uids: In memory of Vladimir P. Skripov," *Int. J. Thermophys.* **31**, 816–830
(2010).
- 931 ⁷⁰J. R. Espinosa, A. Zaragoza, P. Rosales-Pelaez, C. Navarro, C. Valeriani, C.
932 Vega, and E. Sanz, "Interfacial free energy as the key to the pressure-induced
933 deceleration of ice nucleation," *Phys. Rev. Lett.* **117**, 135702 (2016).
- 934 ⁷¹J. Alejandro and G. A. Chapela, "The surface tension of TIP4P/2005 water model
935 using the Ewald sums for the dispersion interactions," *J. Chem. Phys.* **132**, 014701
(2010).
- 936 ⁷²L. J. Briggs, "Limiting negative pressure of water," *J. Appl. Phys.* **21**, 721–722
(1950).
- 937 ⁷³C. Wurster, M. Köhler, R. Pecha, W. Eisenmenger, D. Suhr, U. Irmer, F.
938 Brümmer, and D. Hülser, "Negative pressure measurements of water using the
939 glass fiber optic hydrophone," in *1st World Congress on Ultrasonics* (■, 1995),
940 pp. 635–638.